RSC Advances

ROYAL SOCIETY OF CHEMISTRY

www.rsc.org/advances

RSC Advances

RSCPublishing

ARTICLE

Silver Nanoparticle Aggregates by Room Temperature Electron Reduction: Preparation and Characterization

Cite this: DOI: 10.1039/x0xx00000x

Wei Wang,[a] Manman Yang,[a] Zongyuan Wang,[a] Jinmao Yan,[a] Changjun Liu[a]*

Received ooth January 2012,
Accepted ooth January 2012

DOI: 10.1039/x0xx00000x

www.rsc.org/

A step-by-step room temperature electron reduction has been developed in this work to prepare silver nanoparticle aggregates on anodic aluminium oxide (AAO) substrate. No chemical reducing agent is needed. The aggregates are formed by silver nanoparticles with particle size of about 3 nm. The colour of the silver nanoparticle aggregates can be adjusted from yellow (with small Ag loading) to dark (with high Ag loading). Especially, the colour of these aggregates depends on the size of Ag nanoparticle aggregate, rather than on the size of the single Ag nanoparticle. The silver aggregate/AAO composites show an outstanding surface plasmon resonance (SERS) characteristic. The Raman enhanced factor reaches as high as 1.054×10^7. The silver nanoparticle aggregates can be dispersed as Ag nanoparticles within liquid solution with the removal of the substrate under the assistance of ultrasonic dispersion. The silver nanoparticle aggregates obtained by this step-by-step electron reduction provide us a convenient sustainable storage of metal nanoparticles.

Introduction

Over the past several decades, the synthesis, characteristic and application of noble metal nanoparticles (NPs) have attracted an intense interest.[1-5] Among the noble metal NPs investigated, silver NPs (AgNPs) have shown unique electronic, optical and thermal properties with many applications like catalysis, anti-microbial agents, label-free molecular sensing, chemical imaging and surface enhanced Raman scattering (SERS). Especially, the surface plasmon resonance (SPR) of AgNPs is stronger than that of other noble metal NPs, which makes the preparation and application of AgNPs become a much hotter topic.[6-10] It has been confirmed that the SPR depends on the size, shape and structure of AgNPs, with which the preparation condition has an obvious influence. More recently, there is an increasing interest in the preparation of AgNPs on various substrates like anodic aluminium oxide (AAO).[11,12] The use of such substrates provide us a facile way to tune the nanostructures for a better control of SERS properties. For example, Chang *et al*.[13] reported an *in situ* growth of AgNPs in porous membranes for SERS. The *in situ* growth of AgNPs was performed with electroless-deposited nano seeds on the interior of the membrane, leading to the formation of hot spots and significantly higher SERS enhancement. Gu *et al*.[14] reported a formation of Ag nanorods with optimum length by electrodeposition for the fabrication of hot spots. They confirmed that the nanorod length can be changed by the electrodeposition time. The use of porous alumina membranes as SERS substrates is very promising because of the reasonable cost, easy fabrication and efficient interaction between light and the inner walls of the pores as well as their optical transparency with minimal light absorption and scattering.[15]

Herein, we reported an effective, simple, environmentally-friendly and step-by-step method to fabricate AgNPs on the AAO surface using room temperature electron reduction with argon glow discharge as electron source. Glow discharge is well known as a conventional cold plasma phenomenon with energetic electrons.[16-18] It has been extensively applied for light devices like neon lights and fluorescent lamps. This method needs neither chemical reducing agent nor protective chemical nor the dispersing agent. The influence of chemicals on Ag nanoparticles can be eliminated. With this method, Ag ions are reduced to Ag nanoparticles with small size by electrons firstly and then these silver nanoparticles aggregate together. The characterization using x-ray diffraction (XRD), scanning electron microscope (SEM) and transmission electron microscope (TEM) confirms that silver nanoparticle aggregates are easily formed by AgNPs from the room temperature electron reduction. The silver aggregate/AAO samples possess an outstanding SERS characteristic. The Raman enhanced factor reaches as high as 1.054×10^7.

Experimental Section

Materials and methods

AAO with 0.02 μm in pore size, 0.1 mm in thickness, 13 mm in diameter and 15mg in mass (Whatman International Ltd) was used as the substrate. The silver nanoparticle aggregates were prepared this way: one drop of $AgNO_3$ ethanol solution (5×10^{-4} mol/L; ~ 30 μl) was dropped on the AAO surface. The liquid

spreads out spontaneously. The sample was then put into the center of the glow discharge tube (quartz). After that, the argon glow discharge was initiated. A 3-minute electron reduction was performed. Then the glow discharge was stopped. The sample was removed out to load another drop of $AgNO_3$ ethanol solution. The process was repeated step-by-step for ten steps for all the samples discussed in this paper. Each step includes dropping, loading and electron reduction. The photographs of the whole process are shown in Figure 1. The details of the electron reduction have been reported in previous work.[19] The obtained sample is assigned as Ag/AAO-1. The $AgNO_3$ ethanol solutions with concentrations of 1×10^{-3}mol/L and 5×10^{-3}mol/L were also used. The obtained samples are denoted as Ag/AAO-2 (with 1×10^{-3}mol/L) and Ag/AAO-3 (with 5×10^{-3}mol/L), respectively. The loading of Ag on the single AAO substrate is 0.0162 mg, 0.0324 mg and 0.162 mg for Ag/AAO-1, Ag/AAO-2 and Ag/AAO-3. The corresponding weight percentage is 0.11%, 0.22% and 1.10%.

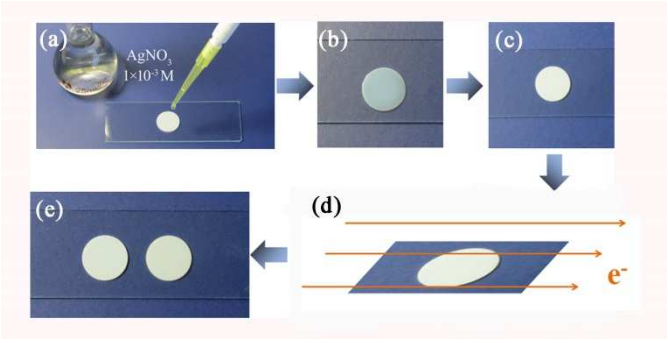

Figure 1. The one step synthesis process of Ag-AAO-2: (a) one drop of the 1×10^{-3} mol/L $AgNO_3$ ethanol solution was dropped on the surface of AAO, (b) the solution spread out, (c) the liquid volatilizes, (d) a 3 minutes electron reduction performed on the sample, (e) the obtained Ag-AAO-2

Characterization

The X-ray diffraction (XRD) patterns of the samples were recorded on a Rigaku D/Max-2500 diffractometer at a scanning speed of 6°/min over the 2θ range of 10–80°. The diffractometer was equipped with a Ni-filtered Cu Kα radiation source (λ=1.54056 Å). The phase identification was made by comparison to the Joint Committee on Powder Diffraction Standards (JCPDSs). X-ray photoelectron spectroscopy (XPS) analyses were performed with a Perkin-Elmer PHI-1600 spectrometer using Mg Kα (hν= 1486.6 eV) radiation. The binding energy (BE) values were calibrated using the C1s peak (hν= 284.6 eV) as reference. High resolution transmission electron microscope (HR-TEM) analyses were performed on a Philips Tecnai G2F20 system operated at 200 kV. The sample was suspended into the ethanol and dispersed ultrasonically for 45 min. A drop of the suspension was deposited on an ultra-thin carbon film. The morphology of the samples was characterized using scanning electron microscope (SEM; FEI Nanosem430). Atomic force microscope (AFM) images were recorded on a multimode SPM and Nanoscope V controller (Veeco Instruments) in the tapping mode with a silicon cantilever. The spring constant and resonant frequency of the cantilever was 30 nm^{-1} and 240 kHz, respectively. UV-vis absorption spectra of the samples were recorded on a Beckman DU-8B UV–Vis spectrophotometer. The surface enhanced Raman spectra (SERS) measurements were collected with a DXR Microscope instrument using a 632.8 nm wavelength He-Ne laser for excitation, with a beam power of 4 mW and integration time of 10s. The size of the spot is about 1.3 μm and a 50× objective with a numerical aperture of 0.5 was used for all measurements.

Results and discussion

Characterization of samples

Figure 2 shows the colour of sample AAO and Ag/AAOs with different Ag loadings. After the electron reduction, the samples show a distinct change in colour. The blank AAO is white. The colour changes to yellow after the AgNPs are formed on the AAO surface. With the increasing loading, the colour changes even to black. The significant colour change indicates the formation of AgNPs on the surface of AAO.[20] In order to make sure if the Ag ion is completely reduced, the XPS analysis was conducted. The results are shown in Figure 3. Characteristic peaks of Al 2s, C 1s and Ag are obviously observed. From Ag/AAO-1 to Ag/AAO-3, the surface composition of Ag is 4.4%, 14.0% and 19.4%, respectively. For samples with different loadings, the surface composition of Ag increases with the increasing concentration of $AgNO_3$ ethanol solution. This suggests that the coverage of AgNPs expands since more AgNPs are formed on the surface. This is consistent with the change of colour, as shown in Figure 2a. Figure 3b, 3c and 3d show the characteristic peaks of Ag in the XPS spectra. For all samples, two symmetrical peaks can be observed. The binding energy of $Ag^0 3d_{5/2}$ is 368.2 eV,[21] while 374.2 eV is assigned to $Ag^0 3d_{3/2}$.[22] These peaks are attributed to Ag^0 with different Ag loadings. The XPS results suggest that Ag ions have been totally reduced into AgNPs by the electron reduction.

Figure 2c shows the UV-vis absorbance spectra of AAO, Ag/AAO-1, Ag/AAO-2 and Ag/AAO-3, respectively. For Ag/AAO-1 and Ag/AAO-2, there is a wide flat peak from 360 nm to 430 nm, which is composed of two peaks at 360 nm and 430 nm. The peak around 430 nm is assigned to the surface plasmon resonance peak of AgNPs.[23] The other one at 360 nm is attributed to Ag_n aggregates,[24,25] which confirms the aggregations of AgNPs. Since the light between 360 nm and 430 nm is absorbed, the colour of Ag/AAO-1 and Ag/AAO-2 is yellow. However, for sample Ag/AAO-3, a flat peak from 300 nm to 800 nm appears, suggesting that the light in the visible region is absorbed. That's why the colour of Ag/AAO-3 is black. However, a new question appears: is the colour change due to the increasing particle size or the aggregation of AgNPs? In order to answer this question, the morphology and structure of AgNPs need to be studied. The wide-angle XRD patterns of the samples are shown in Figure 4. As can be seen in Figure 4, only from patterns of Ag/AAO-3, a little Ag peak is observed at 2θ of 38.24°, assigned to (111) reflection of the face-cantered

cubic Ag crystalline lattice, with the space group attributed toFm-3m(225) (JCPDS card, file No. 65-2871). This suggests Ag ions have been reduced to AgNPs. Other peaks at 2θ of 44.30°, 64.58° and 77.41°, assigned to Ag (200), (220) and (311) reflections, are too small to be seen. For other samples,

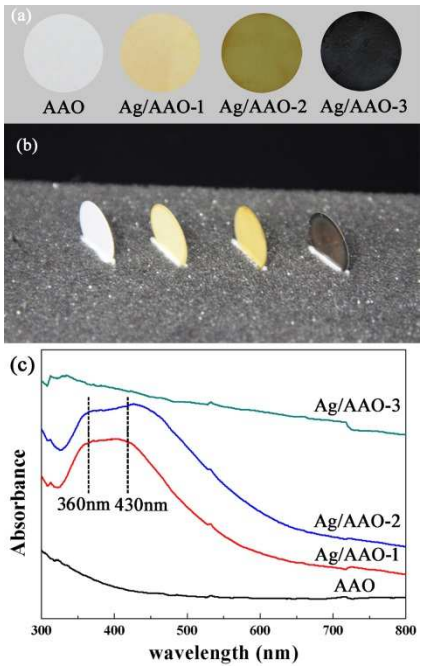

Figure 2. Photographs from (a) the top view, (b) the side view and (c) Uv-vis absorbance spectra of Ag-AAOs with different Ag loadings: AAO, Ag/AAO-1, Ag/AAO-2 and Ag/AAO-3.

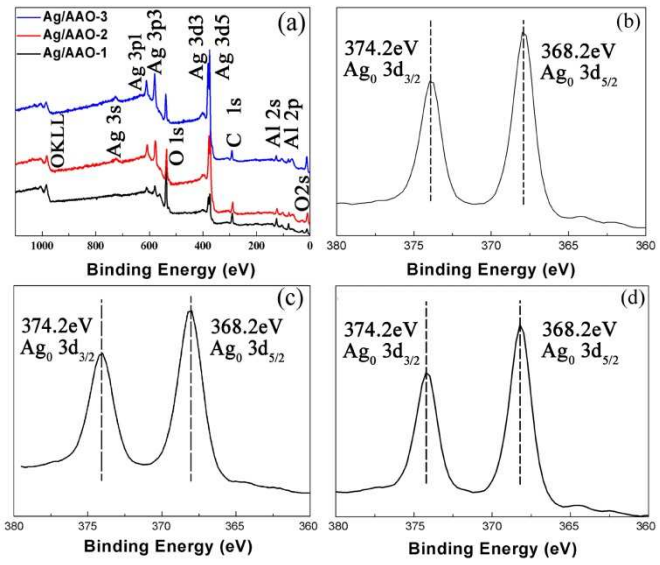

Figure 3. XPS spectra of (a) sample Ag/AAOs and Ag^0 of (b) sample Ag/AAO-1, (c) sample Ag/AAO-2 and (d) sample Ag/AAO-3

no dramatic peaks are found except a very broad peak for amorphous Al_2O_3. There may be three reasons for it: 1) there is no crystalline AgNPs on the AAO surface; 2) the loading of Ag is too low to show peaks; 3) the size of AgNPs is too small to show peaks. The peak in patterns of Ag/AAO-3 indicates the presence of crystalline AgNPs. For Ag-AAO-1 and Ag-AAO-2, the Ag loading is 0.11% and 0.22%, respectively. The Ag loading should be high enough to show peaks in XRD patterns. According to our previous work,[26] we speculate that the reason for no characteristic peaks in the XRD patterns is the small size of AgNPs. In order to confirm this speculation, HR-TEM was employed.

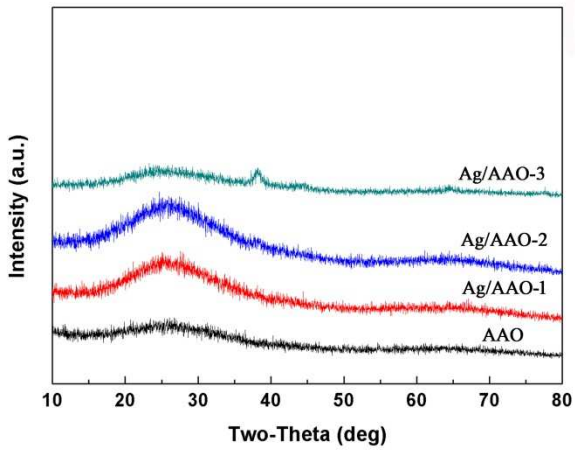

Figure 4. The wide-angle XRD patterns of different samples: AAO; Ag/AAO-1; Ag/AAO-2; Ag/AAO-3

Figure 5 shows HR-TEM images of AAO and Ag/AAOs after ultrasonical dispersion treatment. It can be found that Al_2O_3 without AgNPs in Figure 5a is amorphous. No dramatic particles or defects exist, suggesting that AAO is an appropriate substrate. For Ag/AAOs shown in Figure 5b, 5c and 5d, AgNPs disperse well on the amorphous Al_2O_3, indicating an intense interaction between AgNPs and AAO via the electron reduction.[27] The size of AgNPs of Ag/AAO-1 is about 3 nm, which changes slightly to 5 nm for Ag/AAO-3. Since the electron reduction has an outstanding ability in size control,[19] the increasing size may be due to the coalescence of noble metal NPs by the electron irradiation during the HR-TEM operation.[28,29] This means that the size of AgNPs measured by HR-TEM is larger than that from XRD analysis. However, as observed in Figure 5, even though their size is small, clear lattice fringes of Ag (111) are observed, suggesting that Ag ions have been reduced into AgNPs via the electron reduction in spite of their different colour in Figure 2a.[30] According to the XRD patterns and HR-TEM images, one can find that the size of AgNPs just changes slightly as the Ag loading increases. Therefore the colour change is not from the increasing size of AgNPs.

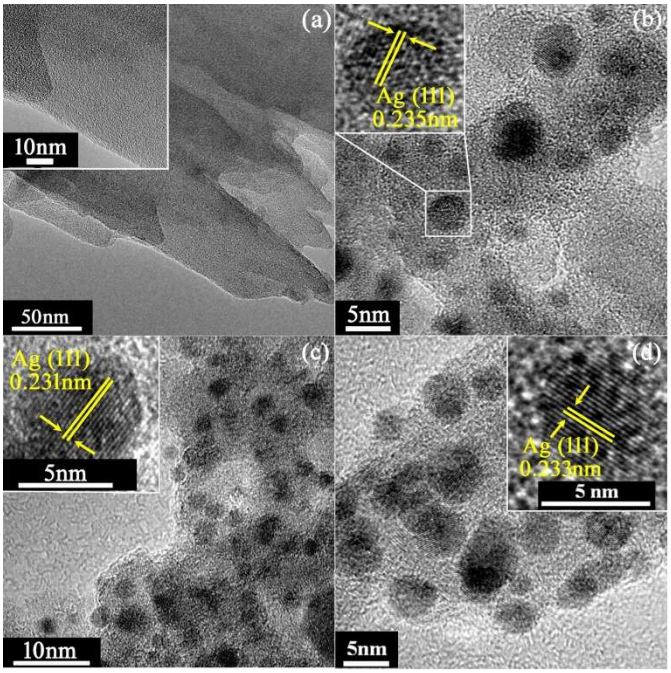

Figure 5. HR-TEM images of different samples: (a) AAO; (b) Ag/AAO-1; (c) Ag/AAO-2; (d) Ag/AAO-3

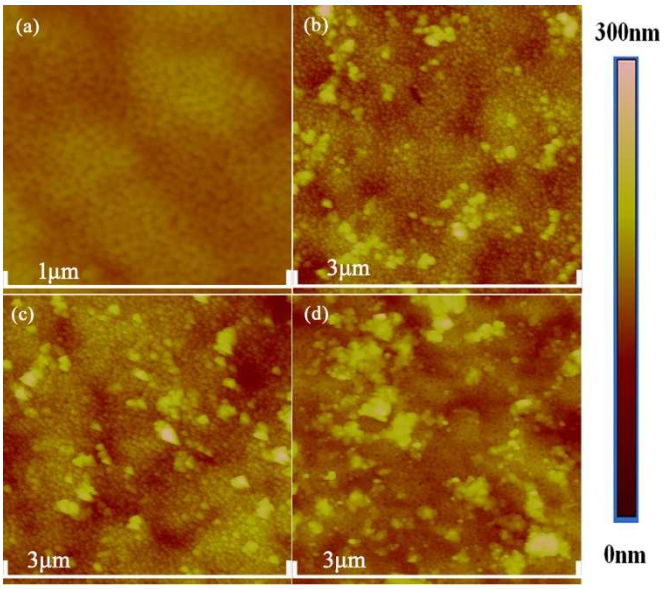

Figure 6. AFM images of different samples: (a) AAO, (b) Ag/AAO-1, (c) Ag/AAO-2 and (d) Ag/AAO-3

Does the aggregation of AgNPs cause the colour change? We need to analyze the aggregation of AgNPs firstly. AFM and SEM images are shown in Figure 6 and Figure 7. From Figure 6a, AAO without AgNPs is flat and full of pores, of which the size is about 20 nm. For samples with AgNPs, it can be observed that the AgNPs aggregate together with irregular morphology and the size of aggregation changes from 20 to 100 nm as the Ag loading increases. This trend can also be found in SEM images shown in Figure 7. These Ag aggregates are formed by AgNPs. The interaction between these small AgNPs is not so strong that the ultrasonically dispersion treatment can make AgNPs well dispersed in the solution. That's why no remarkable peaks can be observed in the XRD patterns even though the size of Ag aggregates is large enough to show remarkable peaks. Ag nanoparticle aggregates are thereby obtained. The aggregation does not proceed through ion-by-ion attachment, but by a particle-mediated process, such as aggregation, on a length scale between 1 nm to 1 μm.[31,32] Even though the traditional Ag nanoparticle aggregation processes need organic additives to form the metal colloid and aggregates,[33,34] we can get Ag nanoparticle aggregates easily through electron reduction directly with no use of organic additives.

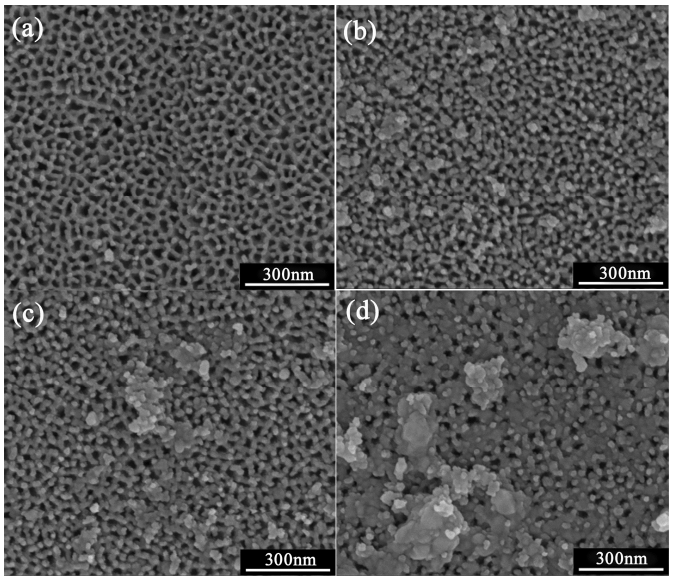

Figure 7. SEM images of different samples: (a) AAO; (b) Ag/AAO-1; (c) Ag/AAO-2; (d) Ag/AAO-3

On the other hand, the main influencing factor on the colour of metal nanoparticles is the SPR, which depends strongly on the size and the shape of metal nanoparticles. When nanoparticles aggregate together, the change of SPR affects the extinction of light and thereby the colour of the particles assembly.[35] For AgNPs (with 20 nm) dispersed well in liquid solution, due to a strong SPR at wavelengths of 410–420 nm, they show a yellow colour. [20,36] With the increasing size, the colour changes from yellow to black. As a theoretical explanation to this colour change, Mie theory is used to precisely calculate the spectra of spherical particles. The calculated extinction and scattering spectra for 50 and 100 nm Ag particles had been given by Hartland.[37] According to his calculation, the 50 nm AgNP has an extinction peak at 410 nm with yellow colour, while the 100 nm AgNP has a wide extinction peak from 350 to 700 nm, showing black colour. These results are consistent with our experimental observation that Ag/AAO-2 with 50 nm aggregations is yellow and the sample Ag/AAO-3 with 100 nm aggregations is black in Figure 2a. That's why samples with

almost the same small size AgNPs show different colours. Obviously, the colour of the Ag/AAO samples depends on the size of aggregates, rather than on the size of single AgNP.

On the basis of the analysis above, we propose the following mechanism for the formation of silver nanoparticle aggregates on the surface of AAO. Firstly, the Ag ions adhere to the surface of AAO. Secondly, the Ag ions are reduced to small AgNPs with about 3 nm via the electron reduction. Finally, during the electron reduction, AgNPs aggregate together on the surface, while the amount and the size of nanoparticle aggregates depend on the loading of Ag. If the loading is large enough, the pores of AAO will be blocked. Large aggregates with hundred nanometers are formed on the surface. Through this aggregation process, the surface area is reduced and therefore the total system energy reduces.[29,38] With different aggregate sizes, Ag/AAOs show different colour. The protective agent and the dispersing agent are not needed with electron reduction. We can also get Ag nanoparticle aggregates with different colours by only changing the concentration of $AgNO_3$ ethanol solution.

SERS of samples

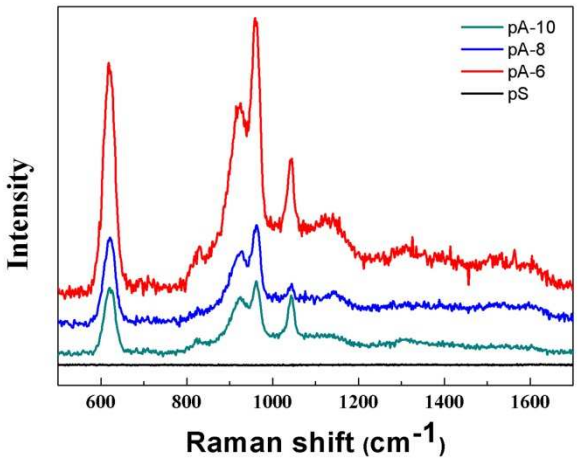

Figure 8. SERS spectra of sample Ag/AAO-3 with Pyridine

Moreover, SERS has been a powerful method to provide structure information in molecular level.[39-41] As AgNPs has been widely studied in SERS, the obtained silver aggregate/AAOs were also tested for SERS spectra. An outstanding SERS characteristic was found. Two samples were prepared. One is to drop a 40 μl pyridine ethanol solution (1×10^{-6} mol/L, 1×10^{-8} mol/L, 1×10^{-10} mol/L) on the surface of Ag/AAO-3. These samples were denoted as pA-6, pA-8 and pA-10, respectively. The other one is the use of 40μl pyridine solution (1×10^{-6} mol/L). This sample was denoted as pS. Figure 8 shows the Raman spectra of pA and pS. The spectra of pA show the characteristic SERS bands for pyridine: ring deformation (617 cm^{-1}) and ring breathing (959 and 1044 cm^{-1}),[42,43] while the Raman spectrum of p-10^{-6} only shows a line without any peaks. The Raman Enhanced Factor (REF) was estimated using the peak intensities of pA-10 and pS in Fig 8 using the following equation:

$$REF = \frac{I_{pA}}{N_{pA}} \times \frac{N_{pS}}{I_{pS}}$$

where I_{pA} and I_{pS} denote the scattering intensities in the pA-10 and pS Raman spectra, respectively, and N_{pS} and N_{pA} represent the amount of pyridine in the spot area, respectively. Here, we employ the band at 959 cm^{-1} to estimate the REF. According to the concentration of the pyridine solution, the value N_{pS}/N_{pA} is 1×10^{4}. The value I_{pA} and I_{pS} are 186.516 and 0.177. So the REF is 1.054×10^{7}. This result indicates Ag/AAOs have an outstanding SERS characteristic.

Conclusions

In conclusion, silver nanoparticle aggregates with different size have been fabricated directly on the surface of AAO substrate at room temperature using electron reduction with argon glow discharge as electron source. This step-by-step method is effective, simple, environmentally-friendly and eliminates the influence of the protective agent and the dispersing agent to AgNPs so that the SPR of AgNPs can be studied directly. With this method, the Ag ions are reduced to AgNPs with small size by the electrons firstly and then these AgNPs aggregate together with different size and different colour. Since the size of silver nanoparticle aggregates can be easily tuned by adjusting the initial $AgNO_3$ concentration and the colour changes simultaneously, we demonstrate that the colour of these samples depends on the size of aggregate, rather than on the size of single AgNP. In addition, these Ag/AAO samples show an outstanding SERS characteristic and the Raman Enhanced Factor is as high as 1.054×10^{7}.

Acknowledgements

This work was supported by the National Natural Science Foundation of China (#91334206).

Notes and references

[a] Collaborative Innovation Center of Chemical Science and Engineering (Tianjin) and School of Chemical Engineering and Technology, Tianjin University, Tianjin 300072, China

1 Y. G. Sun and Y. N. Xia, *Science,* 2002**, 298**, 2176-2179.
2 D. V. Talapin, J. S. Lee, M. V. Kovalenko and E. V. Shevchenko, *Chem. Rev.,* 2009, **110**, 389-458.
3 J. Park, J. Joo, S. G. Kwon, Y. Jang and T. Hyeon, *Angew. Chem., Int. Ed.,* 2007, **46**, 4630-4660.
4 C. J. Liu, U. Burghaus, F. Besenbacher and Z. L. Wang, *ACS Nano,* 2010, **4**, 5517-5526.
5 K. J. Rao and S. Paria, *RSC Adv.,* 2014, **4**, 28645-28652.
6 Z. Q. Tian, B. Ren and D. Y. Wu, *J. Phys. Chem. B,* 2002, **106**, 9463-9483
7 G. S. Hong, C. Li and L. M. Qi, *Adv. Funct. Mater.,* 2010, **20**, 3774-3783.

8 J. M. Yao, A. P. Le, S. K. Gray, J. S. Moore, J. A. Rogers and R. G. Nuzzo, *Adv. Mater.,* 2010, **22**, 1102-1110.
9 J. P. Duan, D. J. Zhao and G. S. Yang, *RSC Adv.,* 2014, **4**, 28765-28768.
10 J. J. Mao, G. F. Zhao, D. S. Wang and Y. D. Li, *RSC Adv.,* 2014, **4**, 25384-25388.
11 P. Pinkhasova, H. Chen, M. W. G. M. Verhoeven, S. Sukhishvili and H. Du, *RSC Adv.,* 2013, **3**, 17954-17961.
12 H. H. Wang, C. Y. Liu, S. B. Wu, N. W. Liu, C. Y. Peng, T. H. Chan, C. F. Hsu, J. K. Wang and Y. L. Wang, *Adv. Mater.,* 2006, **18**, 491-495.
13 S. Chang, Z. A. Combs, M. K. Gupta, R. Davis and V. V. Tsukruk, *ACS Appl. Mat. Interfaces.,* 2010, **2**, 3333-3339.
14 G. H. Gu, J. Kim, L. Kim and J. S. Suh, *J. Phys. Chem. C,* 2007, **111**, 7906-7909.
15 H. Ko and V. V. Tsukruk, *Small,* 2008, **4**, 1980-1984.
16 J. M. Yan, Y. X. Pan, A. G. Cheetham, Y. A. Lin, W. Wang, H. G. Cui and C. J. Liu, *Langmuir,* 2013, **29**, 16051-16057.
17 Q. Chen, T. Kaneko and R. Hatakeyama, *Appl. Phys. Express,* 2012, **5**, 086201.
18 Y. X. Pan, C. J. Liu, S. Zhang, Y. Yu and M. H. Dong, *Chem. Eur. J.,* 2012, **18**, 14614-14617.
19 C. J. Liu, Y. Zhao, Y. Z. Li, D. S. Zhang, Z. Chang and X. H. Bu, *ACS Sustainable Chem. Eng.,* 2014, **2**, 3-13.
20 C. J. Murphy and N. R. Jana, *Adv. Mater.* 2002, **14**, 80-82.
21 M. P. Seah, I. S. Gilmore and G. Beamson, *Surf. Interface Aanl.,* 1998, **26**, 642-649.
22 Y. Liu, R. G. Jordan and S. L. Qiu, *Phys. Rev. B: Condens. Matter Mater. Phys.,* 1994, **49**, 4478-4484.
23 S. Abalde-Cela, S. Ho, B. Rodriguez-Gonzalez, M. A. Correa-Duarte, R. A. Alvarez-Puebla, L. M. Liz-Marzan and N. A. Kotov, *Angew. Chem., Int. Ed.,* 2009, **48**, 5326-5329.
24 K. Shimizu, J. Shibata, H. Yoshida, A. Satsuma and T. Hattori, *Appl. Catal. B,* 2001, **30**, 151-162.
25 T. Linnert, P. Mulvaney, A. Henglein and H. Weller, *J. Am. Chem. Soc.,* 1990, **112**, 4657-4664.
26 Y. Zhou, Z. H. Xiang, D. P. Cao and C. J. Liu, *Chem. Commun.,* 2013, **49**, 5633-5635.
27 Y. Z. Li, Y. Yu, J. G. Wang, J. Song, Q. Li, M. D Dong and C. J. Liu, *Appl. Catal. B,* 2012, **125**, 189-196.
28 J. M. Yuk, M. Jeong, S. Y. Kim, H. K. Seo, J. Kim and J. Y. Lee, *Chem. Commun.,* 2013, **49**, 11479-11481.
29 M. Grouchko, I. Popov, V. Uvarov, S. Magdassi and A. Kamyshny, *Langmuir,* 2009, **25**, (4), 2501-2503.
30 Z. J. Wang, Y. B. Xie and C. J. Liu, *J. Phys. Chem. C,* 2008, **112**, 19818-19824.
31 Z. Liu, X. D. Wen, X. L. Wu, Y. J. Gao, H. T. Chen, J. Zhu and P. K. Chu, *J. Am. Chem. Soc.,* 2009, **131**, 9405-9412.
32 H. Colfen and M. Antonietti, *Angew. Chem., Int. Ed.,* 2005, **44**, 5576-5591.
33 A. W. Xu, M. Antonietti, H. Cölfen, and Y. P. Fang, *Adv. Funct. Mater.,* 2006, **16**, 903-908.
34 A. N. Kulak, P. Iddon, Y. Li, S. P. Armes, H. Cölfen, O. Paris, R. M. Wilson and F. C. Meldrum, *J. Am. Chem. Soc.,* 2007, **129**, 3729-3736.
35 M. Quinten, *Appl. Phys. B: Lasers Opt.,* 2001, **73**, 317-326.
36 T. Huang and X. H. Nancy Xu, *J. Mater. Chem.,* 2010, **20**, 9867-9876.
37 G. V. Hartland, *Chem. Rev.,* 2011, **111**, 3858-3887.
38 J. X. Fang, B. J. Ding and X. P. Song, *Cryst. Growth Des.,* 2008, **8**, 3616-3622.
39 J. F. Li, Y. F. Huang, Y. Ding, Z. L. Yang, S. B. Li, X. S. Zhou, F. R. Fan, W. Zhang, Z. Y. Zhou, D. Y. Wu, B. Ren, Z. L. Wang and Z. Q. Tian, *Nature,* 2010, **464**, 392-395.
40 G. Braun, S. J. Lee, M. Dante, T. Q. Nguyen, M. Moskovits and N. Reich, *J. Am. Chem. Soc.,* 2007, **129**, 6378-6379.
41 P. J. G. Goulet, D. S. dos Santos, R. A. Alvarez-Puebla, O. N. Oliveira and R. F. Aroca, *Langmuir,* 2005, **21**, 5576-5581.
42 D. Y. Wu, J. F. Li, B. Ren and Z. Q. Tian, *Chem. Soc. Rev.,* 2008, **37**, 1025-1041.
43 L. L. Zhao, L. Jensen and G. C. Schatz, *J. Am. Chem. Soc.,* 2006, **128**, 2911-2919.

Graphic Abstract